Heliyon 10 (2024) e26428

Contents lists available at ScienceDirect

Heliyon

journal homepage: www.cell.com/heliyon

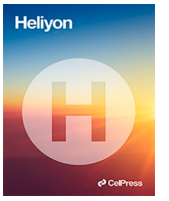

Research article

Assessing energy saving potential of wavelength-dependent passive daytime radiative cooler implemented with EnergyPlus by a roof model

Yujie Yang, Guoqiang Zhang, Li Rong *

Department of Civil and Architectural Engineering, Aarhus University, Inge Lehmanns Gade 10, Aarhus C, 8000, Denmark

ARTICLE INFO

Keywords:
Cooling and heating demand
EnergyPlus
Insulation
Passive daytime radiative cooler
Roof model

ABSTRACT

The Passive Daytime Radiative Cooler (PDRC) exhibits potential in enhancing building energy conservation due to its high emissivity in wavelength between 8 μm and 13 μm. However, current building energy simulation programs, e.g., EnergyPlus, generally adopt a constant emissivity. To implement the wavelength-dependent PDRC model into EnergyPlus, a roof model was introduced to couple it with EnergyPlus to assess the energy saving potential of PDRC more reasonably. To assess the PDRC roofs, the impact of buildings constructed in different eras, building heights, and climatic conditions in China on building energy saving was investigated. The results showed that more energy was saved in regions with high cooling demands e.g., Shanghai and Guangzhou. Applying PDRC on roofs of buildings constructed pre 2001 in severe cold regions increased building energy consumptions. Furthermore, buildings with well insulated roofs coated by PDRC were not equally beneficial for reducing cooling demands in summer compared to buildings with non-insulated roofs, but heating demands in winter could be reduced. With an increase in building height, the energy saving potential of PDRC roofs was reduced. Therefore, a comprehensive analysis was imperative considering the local climates as well as the building itself when PDRC is to be applied.

1. Introduction

Urbanization has led to increased density of buildings and populations, which makes urban areas tend to experience higher temperatures than their surroundings, known as the urban heat island (UHI) effect [1]. Many challenges, such as the concentration of air pollutants, the deterioration of indoor and outdoor thermal comfort, and the increase in building cooling demands, have been raised due to UHI. The research showed that those challenges significantly raise the rate of heat-related mortality and morbidity, exacerbating the living conditions of the vulnerable population in cities [2,3]. To mitigate urban overheating, two commonly investigated strategies are the implementation of urban vegetation and the use of reflective surfaces [4]. Reflective roofs have been applied and studied in the urban context because they can be easily applied in practice [5]. Many states in the USA have already established policies to encourage the use of reflective rooftops through building energy codes or other initiatives. For example, commercial buildings are required a white roof in many American cities [6].

Passive daytime radiative cooler (PDRC), being able to maintain the surface temperature below the ambient air temperatures when

* Corresponding author.
E-mail address: li.rong@cae.au.dk (L. Rong).

https://doi.org/10.1016/j.heliyon.2024.e26428
Received 24 August 2023; Received in revised form 24 November 2023; Accepted 13 February 2024
Available online 17 February 2024

Nomenclature

A_c	opaque sky cover, [−]
A	surface area, [m^2]
C	thermal capacity, [J/K]
c	speed of light in vacuum, 3.0×10^8 [m/s]
c_p	Specific heat, [J/(kg·K)]
F	view factors, [−]
h	Planck's constant, $6.62607004 \times 10^{-34}$ [J·s]
h_c	non-radiative heat exchange coefficient, [W/(m^2·K)]
H	cloud base height, [km]
I	spectral radiance, [W/(m^2·sr m)]
k_B	Boltzmann constant, $1.38064852 \times 10^{-23}$ [J/K]
N	opaque sky cover, [−]
n	fractional area of the sky covered by clouds, [−]
P	radiation flux or power, [W/m^2]
R	thermal resistance, [K/W]
T	temperature, [K]
t	atmospheric transmittance, [−]
x	thickness, [m]
α	absorption coefficient, [−]
ε	emissivity, [−]
σ	Stefan-Boltzmann constant, 5.67×10^{-8} $[W/(m^2K^4)]$
τ	response time, [s]
ρ	density, [kg/m^3]

Abbreviation

AC	Air conditioning
BEM	Building energy model
COP	Coefficient of Performance
DOE	Department of Energy
PDRC	Passive daytime radiative cooler
TMY	Typical meteorological year
UHI	Urban heat island

Subscripts

A	atmosphere
Air	air
BB	black body
Cond	conduction
Conv	convection
C	ceiling
i	inside
LWR	long wave radiation
o	outside
R	passive daytime radiative cooler
Solar	solar
Sun	sun
S	surface

directly exposed to the sun, would further improve the potential of the reflective rooftop to mitigate the UHI [7]. This type of material utilizes the atmosphere window to directly transfer heat to outer space by infrared radiation [8]. A well-designed PDRC can achieve a surface temperature up to 15 ° C lower than the ambient temperature during the daytime, with a net cooling power of more than 100 W/m^2 [9]. Therefore, there is promising potential to utilize PDRC to reduce building cooling demand and it has been considered a viable cooling alternative [10].

One parameter that greatly impacts the performance of the PDRC is climate conditions. Tso et al. [11] used the same PDRC developed by Raman et al. [7] to evaluate the performance of PDRC in Hongkong, but their experiments showed that the cooler's surface temperature was above the surrounding air during the noon, while it was 4.9 ± 5 °C lower than the ambient air temperature in California during the same period [7]. Therefore, the same material could have different performances in different climates. Liu et al.

[12] examined the cooling power of PDRC in various areas of China during the cooling season. The results showed that this value increased gradually from east to west. Yang et al. [13] studied the influence of clouds on the performance of the PDRC. The results showed the difference in annual potential of achieving sub-ambient cooling for the conditions with and without considering the clouds during daytime ranged from 12.68% to 43.35% in five cities in China, which represented five climatic conditions. Since the performance of PDRC is dependent on climate conditions, it is significant to consider this factor when evaluating the strategy of applying the PDRC on the roof.

Another factor that influences the energy-saving potential of PDRC is the intrinsic characteristic of the buildings. Buildings in a city have varied dimensions due to their different functions and have been constructed in different eras. One parameter that can impact the cooling potential of PDRC applied on the roofs is the building height. Feng et al. [14] explored the benefit of applying PDRC on a typical Australian one-story residential building. The results showed that the PDRC roof could save yearly energy consumption by up to 20.6%. However, when it came to multi-story buildings, the yearly energy saving of the PDRC roof ranged from 6% to 13% [15]. Besides, the buildings constructed in different eras have diverse thermal properties of building materials, which have been upgraded with the development of building technologies, the implementation of stricter building regulation codes, as well as the improvement of the energy efficiency of HVAC systems [16]. Applying PDRC to those buildings, the cooling saving potential of PDRC can be varied. Therefore, it is imperative to identify the diverse level of cooling saving potential of applying PDRC on roofs of buildings constructed at different periods when the thermal properties of building materials and energy efficiency of HVAC have been improved.

Serval studies have estimated the impact of applying PDRC on building energy consumption through building energy simulation programs like EnergyPlus [15,17–19]. One method to couple the PDRC with the building energy model (BEM) is to use an equivalent constant emissivity material of which the emissivity is equal to the integral spectral emissivity and its performance can thus be directly simulated by EnergyPlus. Li et al. [20] employed EnergyPlus to calculate the yearly energy saving for midrise apartment buildings in the USA. The results showed that PDRC could save 138 GJ of yearly energy consumption. However, Yu et al. [21] stated that using an equivalent constant emissivity could overestimate the radiative cooling potential by 30.7% compared to the wavelength-dependent emissivity model. Considering the achievement of daytime sub-ambient cooling heavily depends on the atmospheric window between 8 μm and 13 μm, ignoring the wavelength-dependence emissivity of PDRC will lead to certain deviations. Therefore, an appropriate method to couple the wavelength-dependent PDRC model with BEM is critical to reasonably predict its impact on the building energy performance so that its application potential can be reasonably estimated. Considering the PDRC is a layer with some special properties, some methods used for building greenery systems could also be suitable. Dahanayake et al. [22] used an independent building envelope model to couple the greenery system with BEM. Inspired by this approach, a roof model was introduced in this study to couple the wavelength-dependent PDRC model with BEM.

This paper proposed an approach to bridge the wavelength-dependent PRDC model with EnergyPlus by adopting a roof model. This method was then utilized to investigate: (1) the impact of building heights on the potential of applying PDRC on the roofs of residential buildings; (2) the influence of climatic conditions in China on building energy savings when applying PDRC on the roof; and (3) the effects of the roof and wall insulations on the potential of applying PDRC on the roof to reduce energy consumption.

2. Methods

Considering the varied emissivity at different wavelengths of PDRC is not applicable in current EnergyPlus simulations, a method that can couple the PDRC model and EnergyPlus via a roof model was proposed in this section to overcome this challenge. As the roof model was the key to bridging the wavelength-dependent PDRC model with EnergyPlus in this study, choosing a suitable roof model

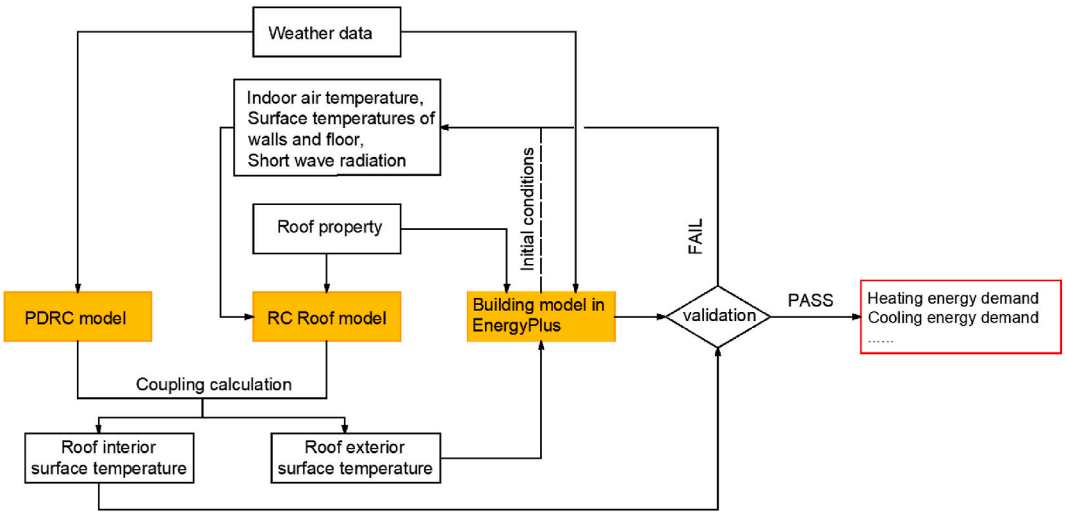

Fig. 1. Flow chart of coupling EnergyPlus and wavelength-dependent PDRC model by the RC roof model.

that can be easily implemented with affordable effort was essential to ensure the success of the coupling between the PDRC model and EnergyPlus. To better understand the coupling process, the coupled process between PDRC and EnergyPlus via the roof model was explained first. The heat transfer processes in which the roof component has been involved were then introduced.

2.1. Coupling the PDRC model with EnergyPlus by an equivalent resistor-capacitor roof model

The process to couple EnergyPlus with the wavelength-dependent PDRC model is outlined in Fig. 1, in which, an RC roof model is introduced to bridge the PDRC model and EnergyPlus so that the wavelength-dependent emissivity can be applied in building energy simulations.

Initially, a building model was created without the application of PDRC on the roof to generate preliminary indoor thermal boundary conditions, which include the surface temperature of internal walls and floors, the indoor air temperature, and indoor shortwave radiation. Subsequently, these values, together with the outdoor climatic conditions obtained from the weather data file, were entered into a RC roof model coupled with a previously validated PDRC model from our prior study [13]. This coupled model was used to calculate the external and internal surface temperatures, accounting for the presence of PDRC on the roof. The resulting outer surface temperatures (T_s) were then employed as the thermal boundary conditions in EnergyPlus simulations.

To ensure the consistency of the thermal boundary conditions between the RC roof model and EnergyPlus, the calculated ceiling surface temperatures (T_c) from the RC roof model were compared to the ceiling surface temperatures ($T_c^{'}$) obtained from EnergyPlus simulations with T_s as the thermal boundary condition. If $\left|T_c - T_c^{'}\right| < 0.1K$, the simulation was considered converged. Otherwise, the process was repeated with the values of the indoor boundary conditions calculated by EnergyPlus in the previous and current steps until convergence was achieved.

2.2. Energy exchange occurred to the roof component

The heat transfer processes within the roof component coated with PDRC are illustrated in Fig. 2, including (1) heat exchange between the external surface of PDRC (arrows marked in solid line) and surroundings, (2) heat conducted within the roof (arrows marked in dotted line), and (3) heat exchange between the internal surface of the roof and indoors (arrows marked in dashed line). Corresponding mathematical models describing the heat transfer processes are presented below.

2.2.1. Equivalent RC model and heat transfer within the roof

As depicted in Fig. 3 (a), a typical roof structure is composed of multiple layers of varying materials. In analogy to the electrical circuit configuration, this intricate arrangement can be represented as a combination of two thermal resistances (R_i and R_o) and a single thermal capacity (C_{Total}), as illustrated in Fig. 3 (b) [23].

After the simplification, the transient heat transfer process can be written in Eq (1):

$$C_{Total}\frac{dT_m}{dt} = \frac{T_s - T_m}{R_0} + \frac{T_c - T_m}{R_i} \tag{1}$$

where T_m (K) is the average temperature of the roof, T_s (K) is the external surface temperature of the roof, which is also the temperature

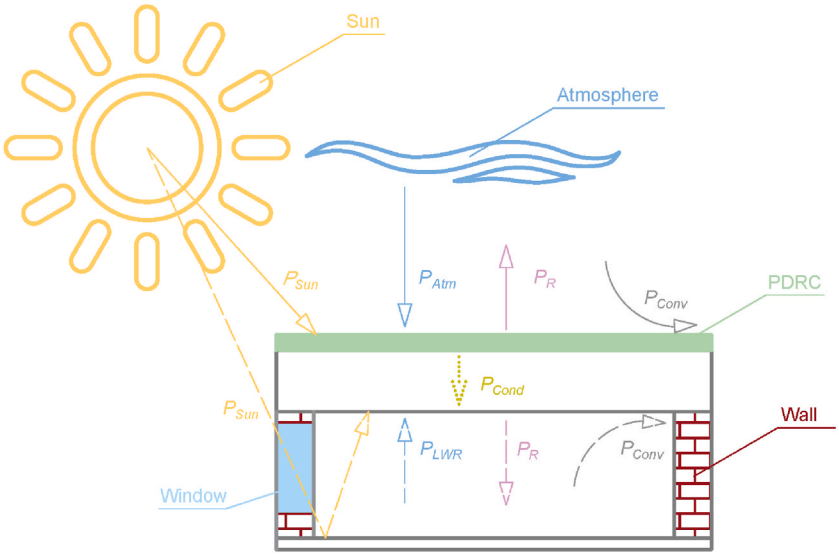

Fig. 2. Sketch of the heat transfer processes between the PDRC roof and its surroundings as well as the heat conduction within the roof.

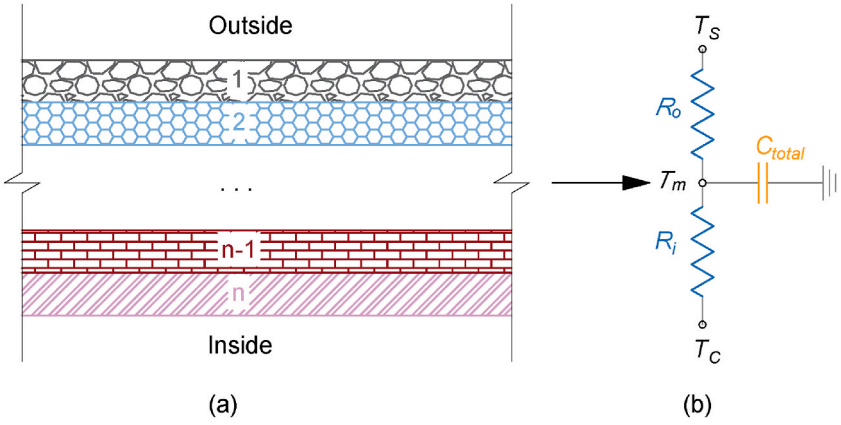

Fig. 3. The equivalent RC circuit of the roof structure.

of the PDRC surface. T_c (K) is the internal surface temperature of roof. To ensure that this simplified structure would capture the response of the roof to external changes, it is vital to reasonably divide the overall thermal resistances into R_i and R_o. This was achieved by employing the Elmore delay model, which was widely used in the electric circuit to simplify the multi-capacitor and resistance electric circuit, to determine the distribution of the thermal resistances [24]. According to the Elmore delay model, the thermal capacity can be calculated by Eq (2)

$$C_{Total} = \mathrm{A}\sum_{i=1}^{i=n}\left(x_i \rho_i c_{p.i}\right) \tag{2}$$

where A (m^2) referres to the area of the roof surface, i denotes the material of the ith layer, x (m) referres to the thickness of materials, ρ (kg/m^3) referres to the density of materials, c (J/(kg·K)) referres to the specific heat of materials.

And R_i and R_o can be calculated by Eq (3) and Eq (4):

$$R_i = \tau_i / C_{Total} \tag{3}$$

$$R_o = \tau_o / C_{Total} \tag{4}$$

where τ_i (s) and τ_o (s) are the response time of the roof to the internal environment and external environment, respectively, and they are calculated by Eq (5) and Eq (6):

$$\tau_o = \begin{cases} C_l \dfrac{R_l}{2} \; for\; l = 1 \\ \displaystyle\sum_{l=1}^{n} C_l \left(\frac{R_l}{2} + \sum_{j=1}^{l-1} R_j \right) \quad for\; l > 1 \end{cases} \tag{5}$$

$$\tau_i = \begin{cases} C_l \dfrac{R_l}{2} \; for\; l = 1 \\ \displaystyle\sum_{l=1}^{n} C_l \left(\frac{R_l}{2} + \sum_{j=l+1}^{n} R_j \right) for\; l > 1 \end{cases} \tag{6}$$

where C_l (J/K) is the thermal capacity of materials in the l th layer, R_l (K/W) and R_j (K/W) are the thermal resistance of materials in l th layer and j th layer, respectively.

2.2.2. *Energy conservation model for external surface of roof*

2.2.2.1. Wavelength-dependent emissivity model. The energy balance of the external surface of the roof can be written as Eq (7):

$$P_R \mathrm{A} + \frac{T_s - T_m}{R_o} = P_{Sun}\mathrm{A} + P_{Atm}\mathrm{A} + P_{Conv.o}\mathrm{A} \tag{7}$$

where P_R (W/m^2) is the radiation released by the external surface of the roof, for the wavelength-dependent emissivity model, it can be calculated by Eq (8):

$$P_R = 2\pi \int_0^{\pi/2} (sin\ \theta)(cos\ \theta) d\theta \int_0^{\infty} I_{BB}(T_S, \lambda)\varepsilon_R(\lambda, \theta) d\lambda \tag{8}$$

P_{Sun} (W/m^2) is the absorbed solar radiation by the external surface of the roof which can be calculated as Eq (9):

$$P_{Sun} = \int_0^{\infty} \varepsilon_R(\lambda, \theta_{Sun}) I_{Solar.s}(\lambda) d\lambda \tag{9}$$

where $I_{Solar.s}(\lambda)$ ((W/(m^2·m))) is solar spectrum.

P_{Atm} (W/m^2) is the atmospheric radiation absorbed by the external surface of the roof obtained by Eq (10):

$$P_{Atm} = 2\pi \int_0^{\pi/2} (sin\ \theta)(cos\ \theta) d\theta \int_0^{\infty} I_{BB}(T_A, \lambda)\varepsilon_R(\theta, \lambda)\varepsilon_A(\theta, \lambda) d\lambda \tag{10}$$

$I_{BB}(T, \lambda)$ (W/(m^2·sr·m)) referres to the wavelength-dependent radiance of a blackbody, for a blackbody with a temperature T (K), its radiance at wavelength λ (m) can be obtained by Eq (11):

$$I_{BB}(T, \lambda) = \frac{2hc^2}{\lambda^5} \frac{1}{e^{hc/(\lambda k_B T)} - 1} \tag{11}$$

with Planck's constant (h, 6.62 × 10^{-34} J s), Boltzmann constant (k_B, 1.38 × 10^{-23} J/K), and the speed of light in vacuum (c, 3.0 × 10^8 m/s), respectively.

$\varepsilon_A(\theta, \lambda)$ is the atmospheric emissivity and can be calculated by Eq (12):

$$\varepsilon_A(\theta, \lambda) = 1 - [1 - \varepsilon_A(0, \lambda)]^{1/cos\ \theta} = 1 - [t(\lambda)]^{1/cos\ \theta} \tag{12}$$

where, $\varepsilon_A(0, \lambda)$ is the atmospheric emissivity at wavelength λ in the normal direction, θ is the angle between the sun and the vertical called the zenith angle. $t(\lambda)$ is the transmittance of the atmosphere in the zenith direction, which can be found in MODTRAN [25].

Clouds can significantly impact atmospheric transmittance. This influence can be determined by Eq. (13) [26]:

$$\varepsilon_A = \varepsilon_{A,0} + \left(1 - \varepsilon_{A,0}\right) \sum_i A_{c,i} \tag{13}$$

where $\varepsilon_{A,0}$ referres to the atmospheric emissivity at the condition of a clear sky, $A_{c,i}$ denotes the opaque sky cover pertaining to the clouds situated at various heights quantified by Eq (14):

$$A_{c,i} = n_i \varepsilon_{C,i} \Gamma_i \tag{14}$$

where n_i is the cloud cover percentage derived from the TMY file, $\varepsilon_{C,i}$ represents the cloud emissivity of the ith height cloud. Γ_i refers to a temperature-dependent factor that can be computationally determined based on the cloud height as in Eq (15):

$$\Gamma_i = \exp(-H_i / H_0) \tag{15}$$

where H_i (km) is the cloud base height for different clouds obtained from weather data file [27], and a constant value (8.2 km) are used for H_0 [26].

ε_R is the emissivity of the PDRC materials. In this study, the material developed by Raman et al. [7] was utilized to investigate the energy-saving potential of PDRC application on building roof. The properties of this material can be found in Section 2.4.1

$P_{Conv.o}$ (W/m2) referres to the convective heat exchange between the external surface of the roof and the surrounding air. This value is computed using Eq. (16):

$$P_{Conv.o} = h_{C.o}(T_A - T_S) \tag{16}$$

where $h_{C.o}$ (W/(m^2·K)) is the convective heat transfer coefficient on the external surface of the roof, which is mainly affected by wind speed v (m/s). This relationship can be quantified in a linear correlation as Eq (17) [28]:

$$h_{C,o} = 3.8v + 5.7 \tag{17}$$

2.2.2.2. Constant emissivity model. In contrast to the wavelength-dependent PDRC model, EnergyPlus utilizes a constant emissivity model for external surfaces of buildings. The energy conservation equation governing the external surface is formulated as Eq (18):

$$P_{Sun.constant} A + P_{LWR.constant} A + P_{conv.o} A = P_{cond} A \tag{18}$$

where $P_{Sun.constant}$ (W/m^2) represents the solar radiation calculated through a fixed solar reflectance and can be determined by Eq (19):

$$P_{Sun} = \alpha I_{Solar} \tag{19}$$

$P_{LWR.constant}$ (W/m^2) denotes the net long wavelength radiation obtained by constant emissivity. For flat roofs, it can be computed using the Eq (20):

$$P_{LWR} = \varepsilon\sigma\left(T_S^4 - T_{Sky}^4\right) \tag{20}$$

with the Stefan-Boltzmann constant (σ, 5.67 $\times$ $10^{-8} W/(m^2K^4)$).

The effective sky temperature T_{Sky} (K) can be determined through Eq (21):

$$T_{Sky} = \varepsilon_{Sky}^{0.25} T_{Air} \tag{21}$$

and the effective sky emissivity ε_{Sky} is related to the dew point temperature T_D (K) and opaque sky cover N obtained from TMY file and can be determined by Eq (22):

$$\varepsilon_{Sky} = (0.787 + 0.764\ln(T_D / 273))\left(1 + 0.0224\mathrm{N} - 0.0035\mathrm{N}^2 + 0.00028\mathrm{N}^3\right) \tag{22}$$

Consequently, EnergyPlus utilizes a constant emissivity model for its external surface. The contrast between the constant emissivity model and the wavelength-dependent emissivity model will be addressed in the subsequent section.

2.2.3. Energy conservation model for ceiling surface

In the case of a hypothetical ceiling surface without thermal mass, the energy balance can be described as Eq (23):

$$\frac{T_m - T_c}{\mathrm{R_i}} = P_{Conv.i}\mathrm{A} + P_{LWR}\mathrm{A} + P_{Sw}\mathrm{A} \tag{23}$$

where $P_{conv.i}$ (W/m^2) is heat exchange between the ceiling and indoor air through convection and can be determined by Eq (24):

$$P_{Conv.i} = h_{C.i}(T_c - T_i) \tag{24}$$

$h_{C.i}$ (W/(m^2·K)) referres to the heat transfer coefficient of convection between the indoor air and the ceiling surface obtained by Eq (25) [29]:

$$h_{C.i} = 3.1(T_c - T_i)^{0.22} \tag{25}$$

P_{LWR} (W/m^2) referres to the heat exchange between the ceiling and indoor surface through infrared radiation calculated by Eq (26):

$$P_{LWR} = \varepsilon_c\sigma\sum F_{c.j}\left(T_c^4 - T_j^4\right) \tag{26}$$

where ε_c referres to the emissivity of the ceiling, $F_{c.j}$ referres to the view factor between the ceiling and other indoor surfaces, mainly including the floor and the walls around it, and T_j (K) referres to the temperature of the corresponding surface that the ceiling views.

For the ceiling and the floor with a size of W and L, separated by a distance of H, the view factor can be calculated by Eq (27) [30]:

$$F_{c.f} = \frac{1}{\pi xy}\left[ln\frac{x_1^2y_1^2}{x_1^2 + y_1^2 - 1} + 2x\left(y_1\ arctan\frac{x}{y_1} - arctanx\right) + 2y\left(x_1\ arctan\frac{y}{x_1} - arctany\right)\right] \tag{27}$$

with $x = W/H$, $y = L/H$, and $x_1 = \sqrt{1 + x^2}$ $y_1 = \sqrt{1 + y^2}$.

For the wall with a size of H and L, the view factor between the ceiling and the wall can be calculated by Eq (28) [30]:

$$F_{c.w} = \frac{1}{\pi w}\left[harctan\frac{1}{h} + warctan\frac{1}{w} - \sqrt{h^2 + w^2}\ arctan\frac{1}{\sqrt{h^2 + w^2}}\right] + 0.25\ ln\left(ab^{w^2}c^{h^2}\right) \tag{28}$$

with $h = H/L$, $w = W/L$. and $a = \frac{(h^2+1)(w^2+1)}{h^2+w^2+1}$, $b = \frac{w^2(h^2+w^2+1)}{(w^2+1)(h^2+w^2)}$, $c = \frac{h^2(h^2+w^2+1)}{(h^2+1)(h^2+w^2)}$.

P_{sw} is short-wave radiation from solar and internal sources (W/m^2) and can be obtained from EnergyPlus.

Table 1
Cooling and heating seasons of the representative cities in China.

Climate zone	Cities	Cooling season	Heating season
Severe cold	Harbin	Jun 12 to Aug 9	Oct 17 to Apr 10
Cold	Beijing	Jun 12 to Sep 2	Nov 12 to Mar 14
Hot summer and cold winter	Shanghai	Jun 19 to Sep 24	Dec 22 to Feb 10
Hot summer and warm winter	Guangzhou	May 6 to Oct 17	–
temperate	Kunming	–	–

2.3. Building energy modeling development in EnergyPlus

2.3.1. Climatic conditions

China is divided into 5 climate zones according to their distinct climate conditions, i.e., the severe cold, cold, hot summer and cold winter, hot summer and warm winter, and temperate climate zone, five Chinese cities, Harbin, Beijing, Shanghai, Guangzhou, and Kunming, were chosen as they encompass a range of climate characteristics that accurately reflect the diverse climate zones across the country. As outlined in Table 1, Harbin, Beijing, and Shanghai experience both heating and cooling demands, with slight difference in heating modes. In the northern region of China, such as Harbin and Beijing, district heating serves as the predominant heating supply system [31], while air conditioning (AC) is the primary heating supply system in the southern part of China, such as Shanghai [32]. For cooling, the multi-split AC is commonly utilized in residential buildings and is the most frequently used air handling unit in urban areas in China [33]. The typical meteorological year (TMY) is adopted as the standard dataset for weather data in building energy simulations.

2.3.2. Archetype of residential buildings

Another important factor to ensure the accuracy of the coupling calculation is to have a suitable BEM that could represent the typical building. Serval studies have built the archetype of buildings and several datasets are available. However, these datasets were usually generated by using a typical building in the USA [34] or Europe [35]. A dataset of an archetype of the residential building in China that can be easily accessed is still missing. In this study, the building standards issued in China were the main reference for determining the typical residential buildings of China.

The buildings with a footprint of 200 m^2 were designed for this study. Following the guidelines outlined by ASHRAE, the floors were divided into five zones, including four perimeter zones that directly connect to the different facade a central core zone [36], as shown in Fig. 4.

The inclusion of thermal characteristics pertaining to building envelopes is essential within the framework of building energy modeling. These values, as reported by Hu et al. [37], have been presented in Table 2. It is shown that the U-value of external envelopes has undergone substantial reduction over the course of time.

Internal heat gains and occupant behavior are other factors that can impact building energy performance. The settings of those factors in EnergyPlus, prescribed by JGJ 134–2001 [38] and JGJ 134–2010 [39], could be found in Table 3. Besides, as these values vary during the day, schedules from the JGJ/T 449–2018 [40] were used to describe the change in occupant behavior, the lighting, and the heat generated by internal equipment during the work days and off-work days.

Heating/cooling set points exert substantial on the cooling and heating demands of buildings. According to GB50736-2012 [41], the cooling setpoint is set as 26 ° C and heating setpoint is and 18 ° C, while they are 24 ° C and 21 ° C in the U.S and European standards, respectively. Besides, the cooling/heating COP (Coefficient of Performance) for AC in different periods was presented in Table 4. It can be seen that the development of technology improved the efficiency of AC. The on-and-off schedules obtained from JGJ/T 449–2018 were used to control the AC's operation in the buildings [40].

The potential energy savings offered by PDRC are influenced by the building categories. The GB50352-2005 [42] has classified buildings into various categories based on their number of floors, including low-rise (1–3), multistory (4–6), middle-high-rise (7–9), high-rise (10–39), and super high-rise buildings (40 floors and above). As the focus of this study is on residential buildings, super high-rise buildings that are generally constructed for commercial purposes have been excluded. The scope of this study encompasses low-rise (3 floors), multistory (6 floors), middle-high-rise (9 floors), and high-rise (18 floors) buildings.

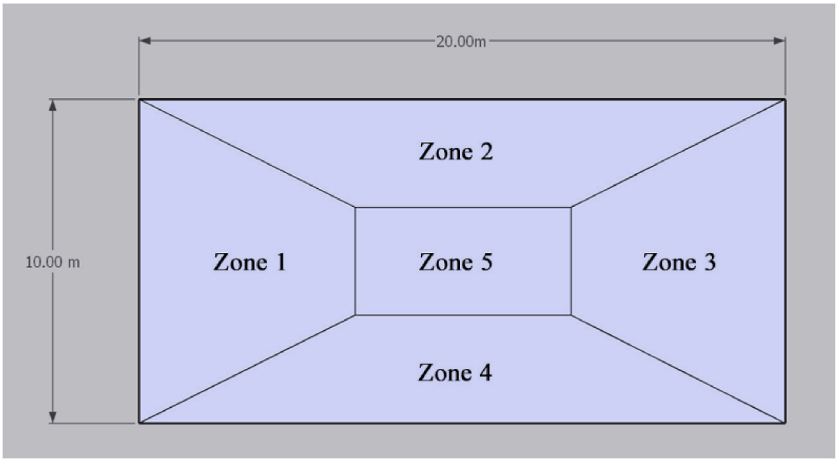

Fig. 4. The footprint of the archetype building and the divide of the thermal zone.

Table 2
Thermal properties of residential buildings built in different periods.

Parameters	Pre-2001	2002–2009	Post-2010
External wall U-value (W/(m^2·K))	1.96	1	0.8
Roof U-value (W/(m^2·K))	1.66	0.8	0.5
Window U-value (W/(m^2·K))	6.6	3.2	2.8
Window Solar Heat Gain Coefficient	0.85	0.48	0.34

Table 3
Parameters set in EnergyPlus related to internal gains.

Parameters	Pre-2001	2002–2009	Post-2010
Lights (W/m^2)	7	7	6
Electric equipment (W/m^2)	4.3		
People (person/m^2)	0.05		

Table 4
Cooling and heating setpoints, and COP of AC.

Parameters	Pre-2001	2002–2009	Post-2010
Cooling/heating setpoints (° C)	26/18		
Cooling/heating COP	2.2/1	2.3/1.9	2.9/2.2

2.4. Model validation

To guarantee the reliability and precision of simulation results, validations were conducted in this study, including the validation of (1) the wavelength-dependent emissivity model, (2) the RC Roof model, and (3) the building energy model. The specific steps undertaken for each validation are described in detail below.

2.4.1. The validation of wavelength-dependent PDRC model

In this study, the data of the PDRC material developed by Raman et al. [7] was utilized for validating the wavelength-dependent emissivity model and assessing the potential of the PDRC application. The emissivity of this material in solar radiation band and long-wave radiation band is depicted in Fig. 5 (a) and Fig. 5 (b), which reveals a low absorption within the solar spectrum range and a pronounced selective emissivity in the atmospheric window. Raman et al. [7] reported that the surface temperature of this PDRC material could be 4.9 °C lower than ambient air when exposed to sunlight. Validation of our PDRC model has been conducted in our previous publication and more details can be found there [13].

2.4.2. RC roof model validation

To assess the capability of the RC roof model to accurately depict temperature variations in the roof due to the change of environmental factors, the procedures proposed in EN ISO 52016 have been followed [43]. In this study, a reference building in EN ISO

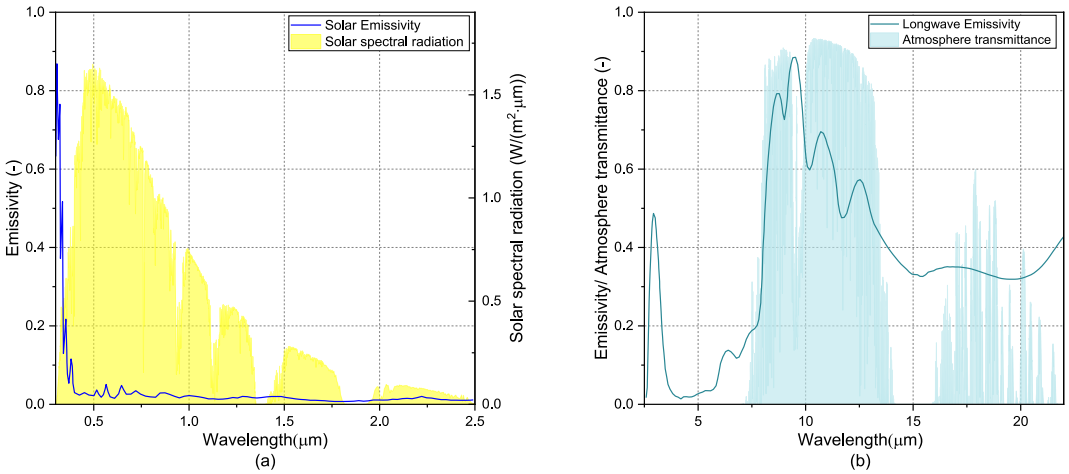

Fig. 5. The emissivity of PDRC material developed by Raman et al. [7] in (a) short wave band and (b) long wave band.

52016 was generated for validation without applying PDRC on the external roof surface, as shown in Fig. 6. The external roof surface temperatures calculated by the RC roof model were compared with results directly calculated by EnergyPlus to verify the rationality of the RC roof model.

The practical Design Manual of Heating and Air Conditioning offers several typical roof structures in China [44]. For the validation, a roof composed of 6 layers with different thicknesses was used, and the specific roof structure is displayed in Fig. 7. The insulation layer was set to a thickness of 50 mm for the validation case. The material properties of each layer used in the roof are summarized in Table 5.

The scenario for validation was set in August in Guangzhou. Therefore, the necessary climatic conditions for calculation were obtained from TMY of Guangzhou. An ideal HVAC system was used in EnergyPlus to maintain the indoor temperature at a constant level of 26 °C. The internal air temperatures, the incident solar radiation, and the necessary wall temperatures were exported from EnergyPlus simulation results and input as the boundary condition for the RC roof model. Then the external roof surface temperatures calculated by the RC roof model and EnergyPlus were compared to examine if the RC roof model could successfully capture the temperature changes in the roof in response to the environmental conditions, which will be further used to bond the wavelength-dependent emissivity model with EnergyPlus.

2.4.3. Validation of BEM in EnergyPlus

Great flexibilities exist in EnergyPlus, as hundreds of parameters could be set in this software, and the simulation results for a given building may differ significantly due to the different assumptions of inputs. Therefore, validation of the BEM is needed to guarantee the reasonableness of the building energy simulation. Compared with the monthly or yearly measured data is the most commonly used method for BEM validation [45]. The yearly energy consumption of a low-rise building constructed post 2010 was calculated by EnergyPlus and then compared to data reported by Deng et al. [46]. The sketch configuration of the building is displayed in Fig. 8, and the set-ups of parameters needed in modeling were introduced in section 2.3.2. Besides, the TMY weather data file was used to provide the climatic conditions for building energy simulations.

To validate the BEM simulations in cold and severe cold climate regions, where the buildings are heated by district heating system, the simulation results were contrast with yearly heating demands defined in GB/T 51161-2016 but not with the results reported by Deng et al. [46] because the energy consumption of the buildings was heated and cooled by AC. If the yearly heating demand simulated in EnergyPlus is under the defined values specified by the standard, it is considered that the BEMs for cold and severe cold regions were reasonable and suitable for further research.

2.5. Summary of simulation cases

The present study involves a diverse set of BEMs with varying parameters to serve different analytical objectives. The BEMs developed in the earlier sections are consolidated in this section to clarify their intended uses. Table 6 presents the BEMs constructed in this study and the corresponding objectives. Firstly, to examine whether the RC roof model can effectively bridge the PDRC model with EnergyPlus, a one-story building conforming to EN ISO 52016 is utilized for RC roof model validation. Subsequently, to ensure that the BEMs developed based on the relevant literature can accurately represent the energy consumption of Chinese buildings, a comparison was made between the estimated energy consumption of low-rise buildings constructed after 2010 by the BEMs and the results reported by Deng et al. [46] and the requirements outlined in GB/T 51161-2016. Thereafter, the impact of climatic conditions, building height, and construction period is examined by deploying different BEMs listed in Table 6. Finally, given that adding insulation is a commonly adopted method to enhance energy efficiency of pre-existing buildings, the combined effect on the application of insulation and PDRC is studied.

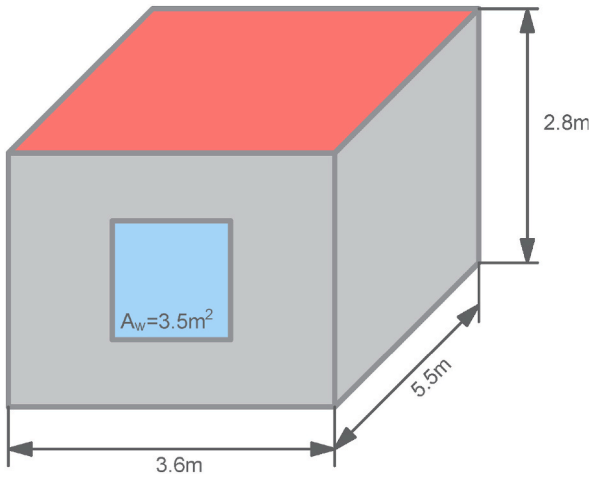

Fig. 6. Schematic of the building proposed by EN ISO 52016 for validation of the RC roof model.

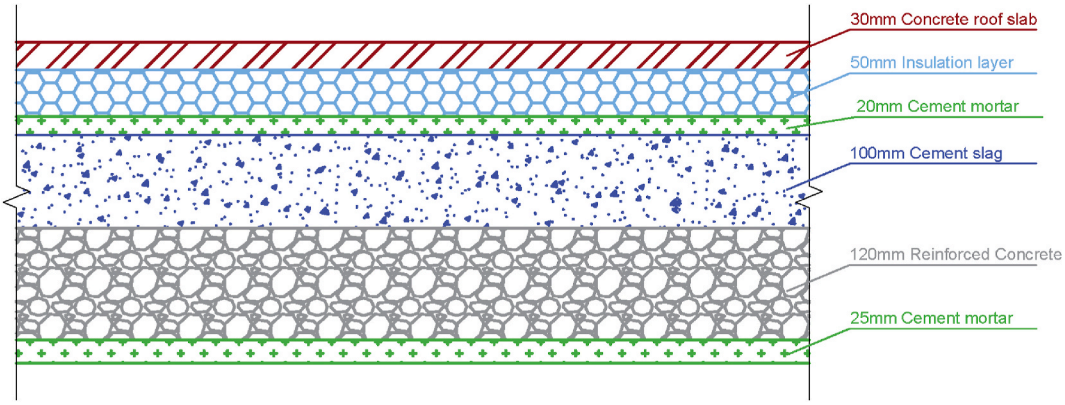

Fig. 7. Building material layers of roof structure used in validation case.

Table 5
Properties of the roof materials.

	Thermal Conductivity (W/(m·K))	Specific Heat Capacity (kJ/(kg·K))	Density (kg/m^3)
Concrete roof slab	0.95	1.05	1700
Insulation	0.042	1.38	30
Cement mortar	0.93	1.05	1800
Cement slag	0.76	1.05	1500
Reinforced concrete	1.54	0.84	2400

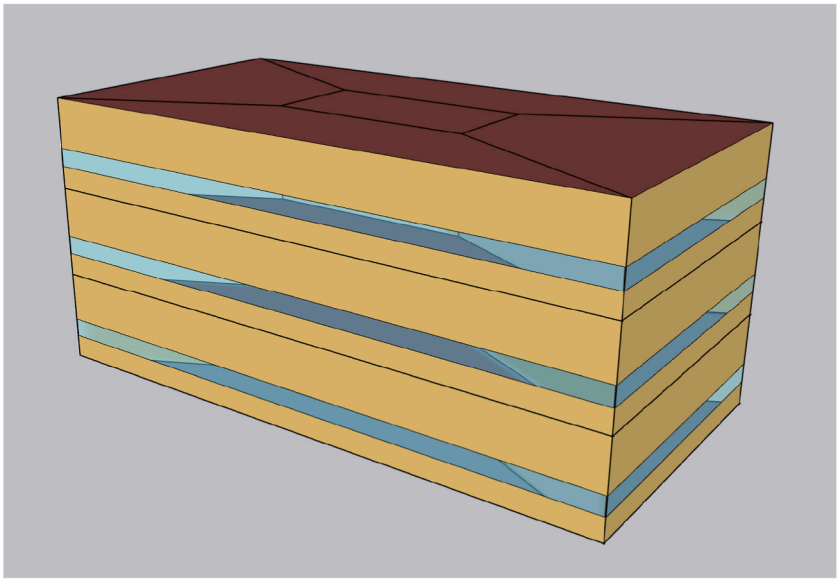

Fig. 8. Schematic of a low-rise building used for validation in EnergyPlus.

3. Results and discussion

3.1. Model validation

3.1.1. Rationalization of the RC roof model

To ensure the validity of the RC roof model, a traditional roof with a reflectance of 0.3 and a constant emissivity of 0.9 are used to compare with the results from EnergyPlus. Fig. 9 shows the external temperature of roof calculated by the RC model and EnergyPlus for Guangzhou in August. It is notable that the external temperature of the roof calculated by the RC model agreed reasonably with the results calculated by EnergyPlus. Therefore, the RC model can capture the temperature change on the roof surface. Fig. 10 also displays

Table 6
Summary of building types used for BEMs.

Purposes		BEM
Roof model validaiton		One-story building in EN ISO 52016
BEM validation		Low-rise building constructed post-2010
Paramatric analysis	Climatic conditions	Low-rise buildings built pre-2001
	Building heights	Pre-2001 buildings with different heights
	Construction era	Low-rise Buildings built in different period
Insulations on the roof		Low-rise buildings constructed pre-2010

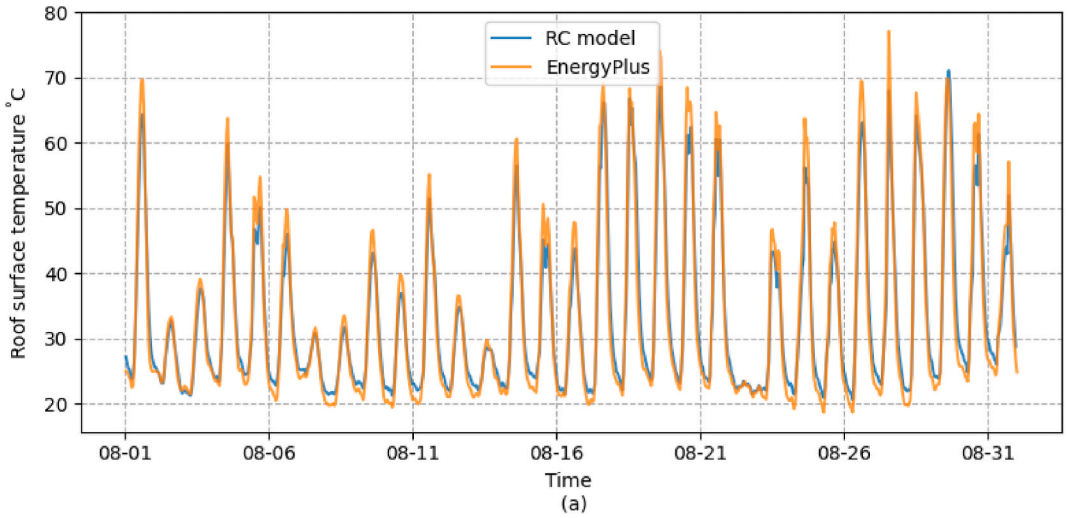

Fig. 9. Comparison of the surface temperature calculated by the RC roof model and EnergyPlus.

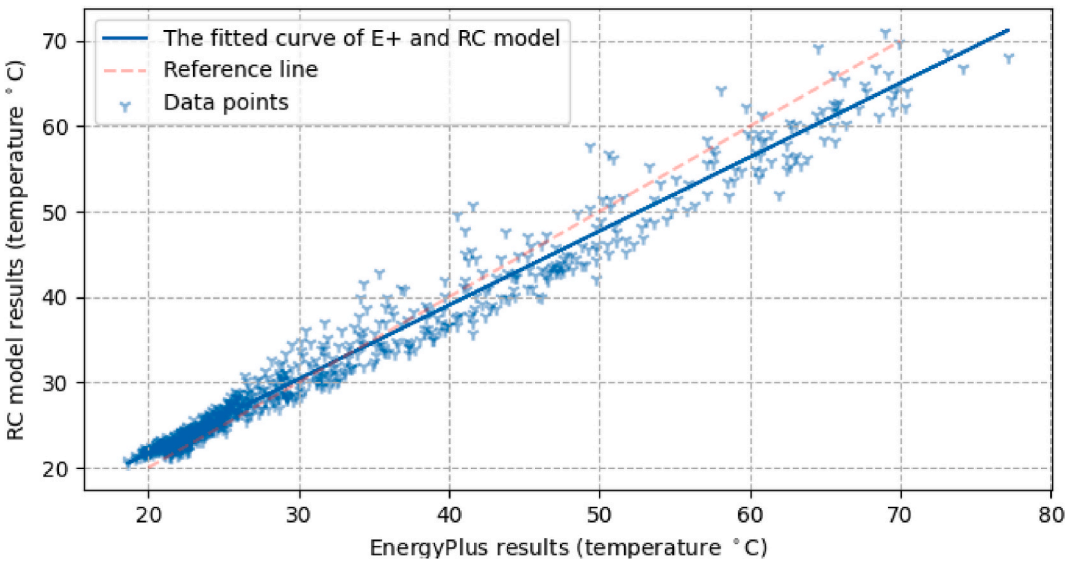

Fig. 10. Correlation of surface temperatures simulated by RC roof model and EnergyPlus.

that the simulated roof external temperature by the RC roof model was highly correlated (R^2 of 0.98) to the ones obtained from simulations conducted in EnergyPlus. Therefore, the RC roof model can reasonably simulate the heat transfer within the roof so that the wave-dependent emissivity can be enabled by using the RC roof model to bridge the coupling of the PDRC model with EnergyPlus.

3.1.2. Building energy model validation

To validate the BEM, the yearly energy consumption of the residential buildings built later than 2010 was calculated. The simulation results in Fig. 11 showed that the buildings' yearly energy consumption in the southern region of China ranged from 35.20 kWh/m^2 to 57.14 kWh/m^2, which matches well with the energy consumption of the residential building summarized by Deng et al. [46], which ranged from 24 kWh/m^2 to 47 kWh/m^2 for measured cases and 39 kWh/m^2 to 46 kWh/m^2 for the simulation cases. For the cold and severe cold region, the heating energy consumption, 102.97 kWh/m^2 and 47.77 kWh/m^2 for Harbin and Beijing, was smaller than the constrained values in GB/T 51161-2016 [47], which were 108.33 kWh/m^2 and 72.22 kWh/m^2 for these two cities. Therefore, the BEMs generated in this study were suitable for further potential analysis of applying PDRC on the roofs of buildings.

3.2. Impact of different parameters associated with residential buildings

3.2.1. Potential of applying PDRC on the low-rise building roof under different climates

The analysis was conducted on a low-rise three-floor building constructed pre-2001. The heating and cooling demands for the building are presented in Fig. 12 (a) and Fig. 12 (b). For two cities in severe cold and cold regions of China, Harbin, and Beijing, AC is still required in summer. Applying PDRC on the roof saved the cooling demand by 0.82 kWh/m^2 in Harbin and 1.69 kWh/m^2 in Beijing. However, its application inevitably increases the yearly heating demand. The heating demand of such a low-rise three-floor building with PDRC applied on the roof was increased by 1.97 kWh/m^2 in Harbin and 0.12 kWh/m^2 in Beijing. Therefore, the application of PDRC on the roof of such a building in Harbin increased the yearly total energy demand by 1.15 kWh/m^2 while decreasing the yearly energy demand in Beijing by 0.70 kWh/m^2. Cities in the temperate region, Kunming, and the hot summer and cold winter region, Shanghai, do not have district heating systems. Therefore, both heating and cooling can only be supplied by AC. The application of PDRC has greater potential in decreasing the cooling demand than in increasing the heating demand in Shanghai. The yearly total energy demand was reduced by 1.31 kWh/m^2 in Shanghai, while in Kunming, the PDRC roof increased the yearly total energy demand by 0.51 kWh/m^2. Given the absence of heating in Guangzhou, the implementation of PDRC on the roof decreased the cooling demand by 2.92 kWh/m^2.

The change in the building energy consumption is mainly due to the cooling potential of PDRC, leading to significantly lower external surface temperature as shown in Fig. 13 (a). The external surface temperature was reduced up to 21.38 °C compared to the one with the traditional roof. Such large temperature reduction thus decreased the energy demand for low-rise buildings in Guangzhou. Fig. 13 (b) shows the changes in the external surface temperature over a day. A large temperature difference is observed during the daytime, and the peak of the external surface temperature difference occurred at 13: 00, the time with the largest solar radiation. However, the temperature of the roof external surface exhibited a close resemblance between the PDRC roof and the traditional roof during the night because solar radiation was not available.

3.2.2. Influence of building heights on energy saving ratio of PDRC roof

Fig. 14 shows the influence of building heights on the energy saving ratio achieved by using PDRC roofs in comparison to traditional roofs, for low-rise buildings in Shanghai. The reason that Shanghai was selected in those simulations is that both cooling and heating are needed in Shanghai. Because the ratio of the roof to the building's external surface decreases with building height, the energy-saving ratio was reduced with an increase in building height. For the low-rise building, applying PDRC on the external surface of the roof could save cooling demand by 13.81%, while for high-rise buildings, this ratio was only 1.77%. The heating penalty decreased slightly with the increase in building height as the energy saving ratio of the heating is −1.36% for the low-rise building and −0.26% for the high-rise building. Therefore, the application of PDRC for low-rise buildings would have a larger influence on the energy-saving potential of cooling than increased energy demand of heating. This can be explained by the performance of PDRC in different seasons.

Fig. 15 shows the external surface temperature of the roof in summer and winter for the low-rise buildings constructed pre-2001 in

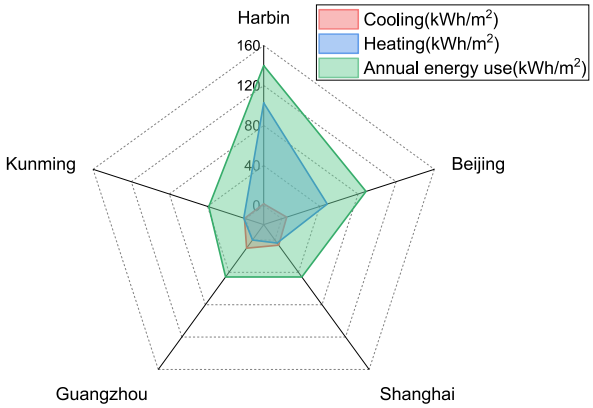

Fig. 11. The energy use of the low-rise buildings built post-2010 in Harbin, Beijing, Shanghai, Guangzhou, and Kunming.

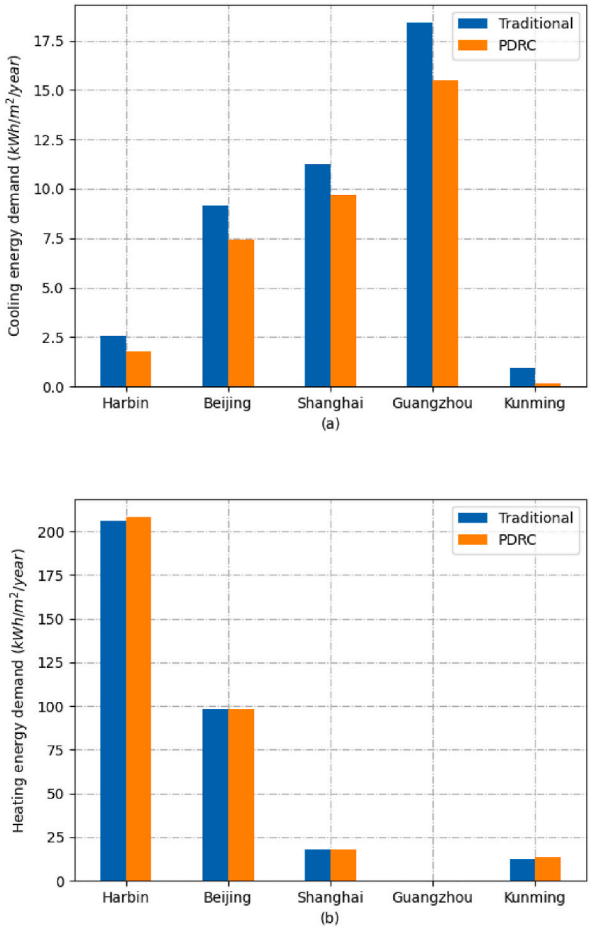

Fig. 12. The predicted (a) heating and (b) cooling demand of buildings constructed pre-2001 with PDRC and traditional roofs in Harbin, Beijing, Shanghai, Guangzhou, and Kunming.

five cities. According to Fig. 15 (a), the average external surface temperature differences between PDRC and traditional roofs were 4.12 °C in Harbin, 4.71 °C in Beijing, 3.72 °C in Shanghai, 4.45 °C in Guangzhou, and 5.36 °C in Kunming. In winter, according to Fig. 15 (b), the mean external surface temperature differences between PDRC and traditional roofs were 0.66 °C, 0.59 °C, 0.42 °C, 1.65 °C and 0.91 °C for low-rise buildings in Harbin, Beijing, Shanghai, Guangzhou, and Kunming, respectively. This variation can be explained by the varying efficiency of PDRC under different climatic conditions, especially due to the fluctuation in atmospheric water content and solar radiation throughout the year [13]. Overall, PDRC as a passive cooling strategy on the roof will only result in less than 1 % change in energy consumption of high-rise buildings. Applying PDRC on the roofs of high-rise buildings may not be a suitable solution for saving energy consumption.

3.2.3. Energy saving potential of PDRC roof for buildings constructed at different periods

The thermal properties of building materials have been improved to reduce the energy consumption of buildings, as well as the energy efficiency of the HVAC system inside the buildings. These improvements impact the potential of PDRC to save energy. Fig. 16 shows the energy consumption of a three-floor low-rise building constructed at different periods in Shanghai. Applying PDRC on the roof of this three-floor low-rise building slightly increased the heating demand and moderately decreased the cooling demand for buildings constructed at any period. More specifically, the heating energy demands for buildings constructed pre 2001, 2002 to 2009, and post 2010 increased by 0.24 kWh/m^2, 0.03 kWh/m^2, and 0.01 kWh/m^2, respectively, while the cooling energy demand decreased by 1.55 kWh/m^2, 0.87 kWh/m^2 and 0.47 kWh/m^2. Therefore, the application of PDRC would reduce the yearly demand by 1.31 kWh/m^2, 0.84 kWh/m^2, and 0.45 kWh/m^2 for buildings built pre 2001, 2002 to 2009, and post 2010, respectively. Besides, a sharp decrease appeared in the heating energy demand when it comes from the buildings built pre 2001 to the buildings built between 2002 and 2009, as it is shown in Fig. 16. This is because, on the one hand, the thermo-physical properties of the building envelope have been greatly improved, as U-value decreases from 1.66 W/(m^2·K) to 0.8 W/(m^2·K), on the other hand, the energy coefficient of the HVAC system has also been significantly improved, as the heating COP increases from 1.0 to 1.9.

Fig. 17 displays the yearly energy savings resulting from the application of PDRC on building roofs, constructed at different periods

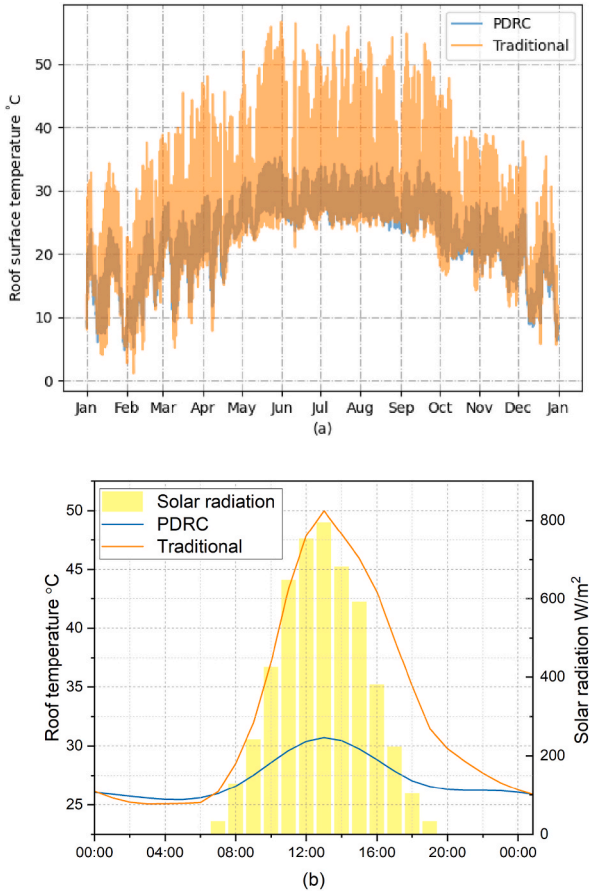

Fig. 13. The predicted external surface temperature of the PDRC and traditional roof in Guangzhou (a) for the whole year and (b) on July 30.

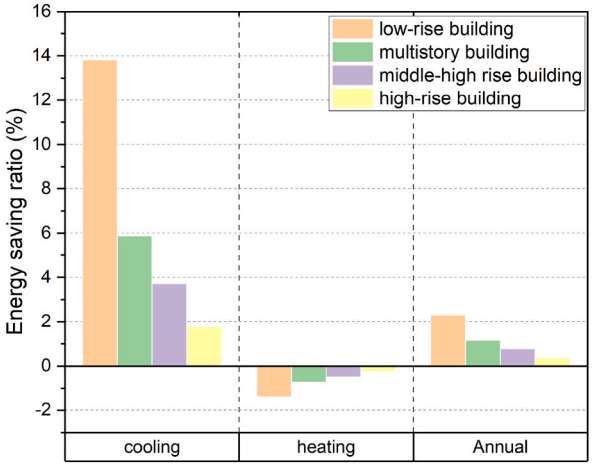

Fig. 14. The energy saving ratio of the PDRC roof for buildings with different heights in Shanghai.

in five Chinese cities. Applying PDRC on the roof will decrease the yearly energy consumption except for the buildings constructed pre 2001 in Harbin and Kunming, due to the relatively poor thermal properties of the building envelope and the relatively low efficiency of the HVAC system. Besides, the application of PDRC will benefit most of the buildings built pre 2001 in Beijing, Shanghai, and Guangzhou, with a yearly energy saving of 1.80 kWh/m^2, 1.31 kWh/m^2, and 2.92 kWh/m^2. Due to the extremely cold weather in Harbin, the improvement of building standards on thermal insulation can effectively reduce the heating demands of buildings.

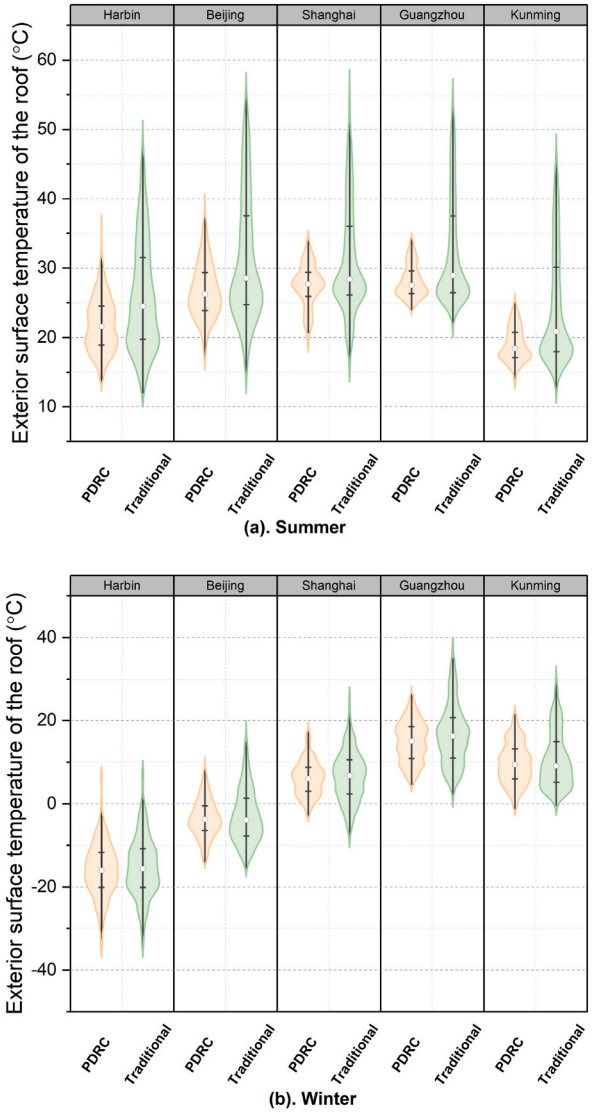

Fig. 15. Comparison of external surface temperature between PDRC and traditional roofs of a three-floor low-rise building in (a) summer and (b) winter at Harbin, Beijing, Shanghai, Guangzhou, and Kunming.

Therefore, the application of PDRC would save 0.20 kWh/m^2 energy for buildings constructed post 2010 in Harbin.

3.3. Influence of insulation on the potential of applying PDRC

3.3.1. Roof insulation

The cooling demands influenced by the thickness of the insulation material applied for the roof element are presented in Fig. 18 by adopting a low-rise building. According to Fig. 18 (a), with the insulation thickness increasing from 0 mm to 70 mm, for the roof with PDRC, the cooling demand increased from 1.76 kWh/m^2 to 2.21 kWh/m^2 in Harbin, from 7.42 kWh/m^2 to 7.84 kWh/m^2 in Beijing, from 9.66 kWh/m^2 to 9.89 kWh/m^2 in Shanghai, from 15.43 kWh/m^2 to 15.69 kWh/m^2 in Guangzhou and 0.16 kWh/m^2 to 0.55 kWh/m^2 in Kunming. But for the traditional roof, According to Fig. 18 (b), the cooling demand decreased from 2.58 kWh/m^2 to 2.44 kWh/m^2 in Harbin, from 9.14 kWh/m^2 to 8.28 kWh/m^2 in Beijing, from 11.24 kWh/m^2 to 10.30 kWh/m^2 in Shanghai, from 18.41 kWh/m^2 to 16.44 kWh/m^2 in Guangzhou and 0.94 kWh/m^2 to 0.89 kWh/m^2 in Kunming. These distinct phenomena could be explained by two factors. First, due to the strong cooling effect of PDRC, its external surface temperature remains lower than the ambient environment during most of the daytime, thereby serving as a cooling source for the building. The addition of insulation reduces the potential of reducing the cooling demand provided by PDRC. Secondly, as the study targets residential buildings, people usually stay in their workplace rather than at home during the daytime, resulting in low power operation of the HVAC system. The combination of these two effects results in an increase of cooling energy demand with increasing insulation thickness for PDRC roofs. However, in the case of

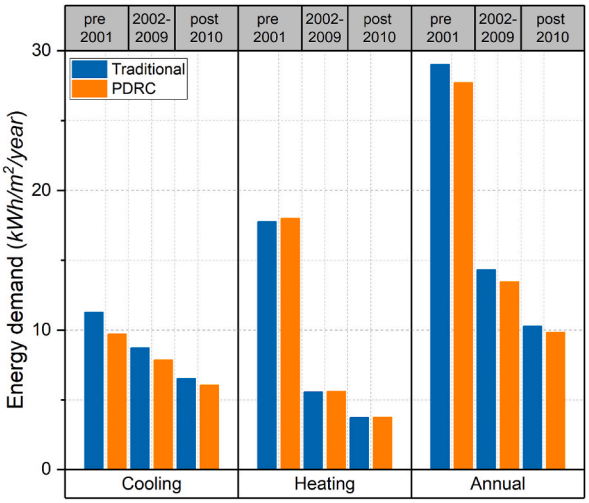

Fig. 16. Energy demand of the buildings constructed pre 2001, from 2002 to 2009, and post 2010 in Shanghai.

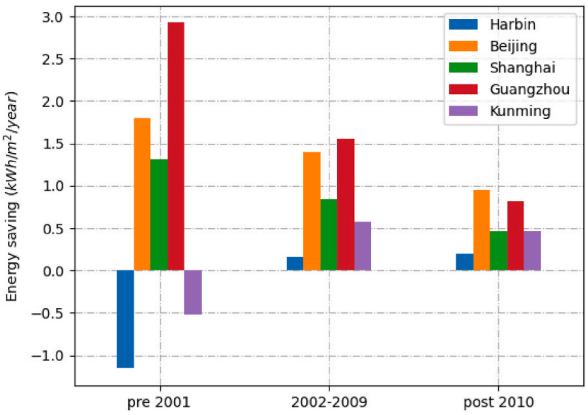

Fig. 17. Yearly energy saving of PDRC roof for a three-story building constructed pre 2001, from 2002 to 2009, and post 2010 in Harbin, Beijing, Shanghai, Guangzhou, and Kunming.

conventional roofs, where the surface temperature significantly exceeds the ambient air temperature under solar exposure, the addition of an insulation layer effectively inhibits heat transfer from the warm external roof surface to the interior space. As a result, this insulation mitigates the cooling demand of buildings.

Fig. 19 shows the heating energy demand for the buildings with different insulation layers in the roofs. Compared to the cooling demand, adding insulation has a consistent influence on the heating demand of buildings. The results demonstrate that the 70 mm insulation reduced the energy consumption of buildings with PDRC roof by 19.13% for Harbin, 20.57% for Beijing, 20.13 % for Shanghai, and 33.71 % for Kunming, compared to the energy consumption of buildings without insulation, according to Fig. 19 (a). For the traditional roof with 70 mm insulation, according to Fig. 19 (b), the heating demand decreased by 18.37%, 20.34 %, 19.40%, and 28.45% for these five cities, respectively.

While the presence of insulation layers in PDRC roofs may lead to a slight increase in cooling demand, their impact on reducing heating demand is substantial. With the exception of Guangzhou, a city that does not require heating, the utilization of a 70 mm thickness on PDRC roofs results in a decrease in yearly energy demand. Specifically, for Harbin, the reduction amounts to 39.42 kWh/m^2, while for Beijing, it is 19.82 kWh/m^2. Similarly, in the case of Shanghai and Kunming, the energy demand decreases by 3.37 kWh/m^2 and 4.24 kWh/m^2, respectively.

Besides, the insulation affects the conduction from the roof external surface to the indoor environment, its thickness will thus impact the roof surface temperature. Fig. 20 shows the yearly average temperature difference between the roofs with different insulation thicknesses and without insulation. It can be seen that this surface temperature difference increased with the increase of the insulation thickness. The magnitude of the impact also varies with climatic conditions. As Guangzhou has the highest outdoor air temperature yearly around (average value of 23.16 ° C), adding 70 mm insulation will only decrease the external surface temperature by 0.07 ° C, while in Harbin, a city in the coldest region of China, the same insulation will reduce the surface temperature by 0.678 ° C.

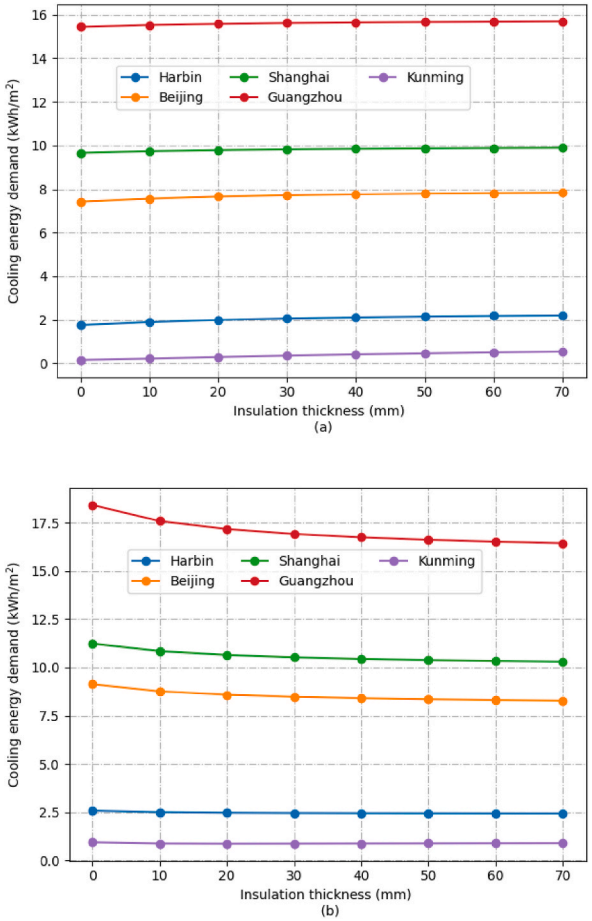

Fig. 18. Influence of roof insulation thickness on cooling demand with (a) PDRC roof and (b) traditional roof in Harbin, Beijing, Shanghai, Guangzhou, and Kunming.

3.3.2. Wall insulation

Another parameter that will impact the performance of the building's energy consumption is the thermal property of the wall. Considering the wall's thermal properties will not directly impact the performance of the PDRC roof, we therefore only discuss the cases with the PDRC roof.

As shown in Fig. 21, the increase in the wall insulation thickness, compared to the increase in roof insulation thickness, will have a greater influence on the building's energy consumption. Specifically, according to Fig. 21 (a), in Harbin, the cooling demand is reduced by 0.044 kWh/m^2, while in Beijing, it decreases by 2.18 kWh/m^2. In Shanghai, the cooling demand is lowered by 2.43 kWh/m^2, whereas in Guangzhou, the reduction is 4.22 kWh/m^2. In Kunming, the cooling demand diminishes by 0.059 kWh/m^2. On the other hand, according to Fig. 21 (b), the heating demand experiences substantial decreases across all cities. In Harbin, it is reduced by 88.84 kWh/m2, in Beijing by 42.07 kWh/m^2, in Shanghai by 7.76 kWh/m^2, and in Kunming by 6.84 kWh/m^2. In contrast, the corresponding reductions in heating and cooling demands for the roof are much smaller. Given that the wall constitutes the majority of the building envelope area, occupying 73.27% of the area for three-story buildings, it serves as the primary interface between the indoor and outdoor environments. In practice, applying PDRC on vertical façades can cause glare issues due to its high reflectance. The application of PDRC on vertical façades would be feasible only if these issues could be addressed.

4. Conclusion

This study presents an approach for integrating the wavelength-dependent PDRC model with BEM of EnergyPlus. As the performance of the PDRC heavily relies on its own wavelength-dependent emissivity as well as the atmospheric emissivity, this method can enable the inclusion of these two parameters in our modelling, which are not allowed by default in EnergyPlus. Besides, this method also enables the heat conduction through the roof layers to be modelled, which has not been simulated in the conventional PDRC model. We believe this coupling method can provide better prediction of PDRC potential in building energy saving.

The external surface temperature of PDRC roofs is obviously lower than traditional roofs, which indicates PDRC roofs function as a cooling source of buildings. It is clear that PDRC applied on roofs of high-rise buildings has neglected impact on energy savings and it is

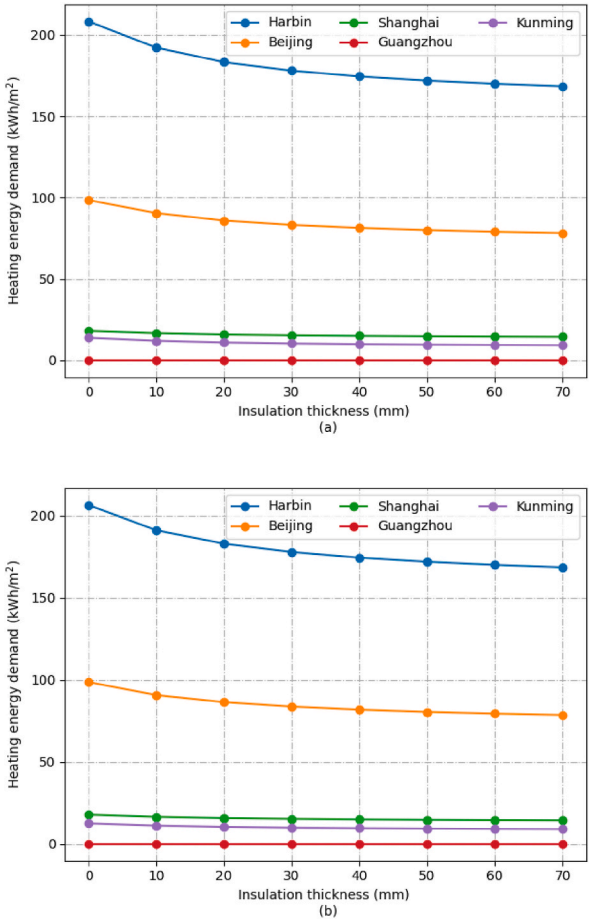

Fig. 19. Influence of roof insulation thickness on heating demand with (a) PDRC roof and (b) traditional roof in Harbin, Beijing, Shanghai, Guangzhou, and Kunming.

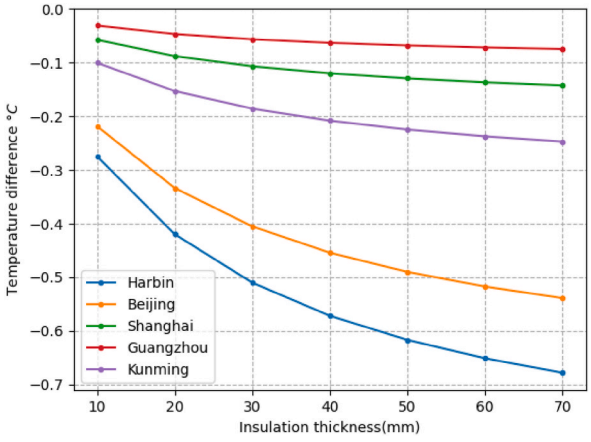

Fig. 20. Influence of the roof insulation thickness on the PDRC roof surface temperature in Harbin, Beijing, Shanghai, Guangzhou, and Kunming.

more promising to apply PDRC on the roof of low-rise buildings. The potential of PDRC in yearly energy savings varies with buildings constructed in different eras, mainly influenced by the improved thermal properties of building materials in newer buildings and the enhanced COP of HVAC systems too. The potential of PDRC in energy savings is also influenced by climatic conditions and is efficient in reducing the cooling demand in Beijing, Shanghai and Guangzhou while this influence would be weakened in newer buildings in

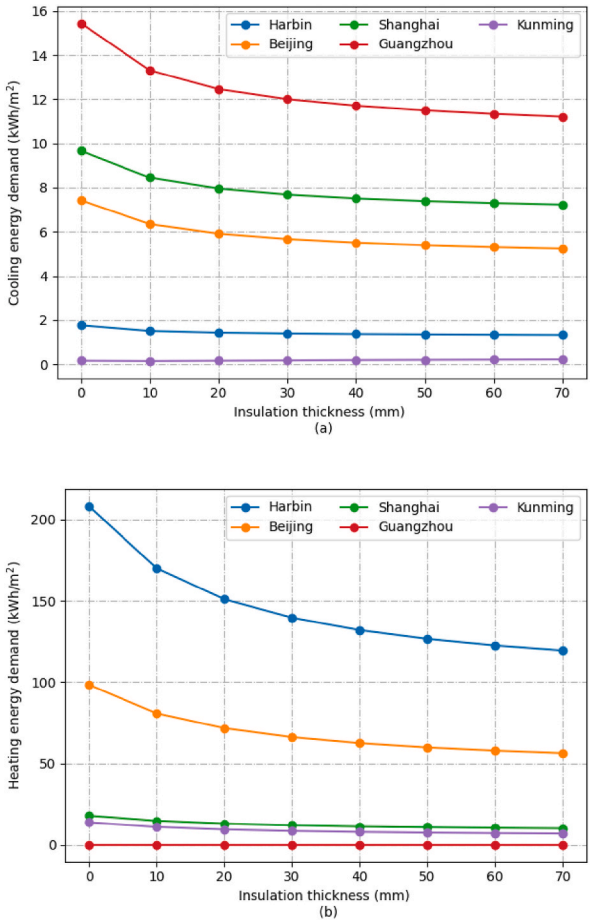

Fig. 21. Influence of the wall insulation thickness on (a) cooling demand and (b) heating demand for buildings with PDRC roof in Harbin, Beijing, Shanghai, Guangzhou, and Kunming.

those climates. Insulation thickness on the PDRC roof could negatively impact the potential of PDCR in saving cooling demand but generally has a positive effect on yearly energy savings. Applying PDRC on building walls can generate higher potential, but issues such as glare should be carefully considered.

Data availability statement

Data associated with this study has not been deposited into a publicly available repository and data will be made available on request.

CRediT authorship contribution statement

Yujie Yang: Data curation, Formal analysis, Funding acquisition, Investigation, Methodology, Validation, Visualization, Writing – original draft, Writing – review & editing. **Guoqiang Zhang:** Conceptualization, Funding acquisition, Supervision, Writing – review & editing. **Li Rong:** Conceptualization, Funding acquisition, Methodology, Project administration, Supervision, Writing – original draft, Writing – review & editing.

Declaration of competing interest

The authors declare that they have no known competing financial interests or personal relationships that could have appeared to influence the work reported in this paper.

Acknowledgments

The first author is partly supported by China Scholarship Council (CSC).

References

[1] M. Santamouris, Regulating the damaged thermostat of the cities—Status, impacts and mitigation challenges, Energy Build. 91 (2015) 43–56, https://doi.org/10.1016/j.enbuild.2015.01.027.
[2] N.B. Grimm, S.H. Faeth, N.E. Golubiewski, C.L. Redman, J. Wu, X. Bai, et al., Global change and the Ecology of cities, Science 319 (2008) 756–760, https://doi.org/10.1126/science.1150195.
[3] M. Santamouris, C. Cartalis, A. Synnefa, D. Kolokotsa, On the impact of urban heat island and global warming on the power demand and electricity consumption of buildings—a review, Energy Build. 98 (2015) 119–124, https://doi.org/10.1016/j.enbuild.2014.09.052.
[4] A.M. Rizwan, L.Y.C. Dennis, C. Liu, A review on the generation, determination and mitigation of Urban Heat Island, J. Environ. Sci. 20 (2008) 120–128, https://doi.org/10.1016/S1001-0742(08)60019-4.
[5] O. Aleksandrowicz, M. Vuckovic, K. Kiesel, A. Mahdavi, Current trends in urban heat island mitigation research: Observations based on a comprehensive research repository, Urban Clim. 21 (2017) 1–26, https://doi.org/10.1016/j.uclim.2017.04.002.
[6] EPA, Heat Island Community Actions Database, United States Environmental Protection Agency n, d, 2018.
[7] A.P. Raman, M.A. Anoma, L. Zhu, E. Rephaeli, S. Fan, Passive radiative cooling below ambient air temperature under direct sunlight, Nature 515 (2014) 540–544, https://doi.org/10.1038/nature13883.
[8] J. Chen, L. Lu, Development of radiative cooling and its integration with buildings: a comprehensive review, Sol. Energy 212 (2020) 125–151, https://doi.org/10.1016/j.solener.2020.10.013.
[9] M.M. Hossain, M. Gu, Radiative cooling: principles, progress, and potentials, Adv. Sci. 3 (2016) 1500360, https://doi.org/10.1002/advs.201500360.
[10] X. Lim, The super-cool materials that send heat to space, Nature 577 (2019) 18–20, https://doi.org/10.1038/d41586-019-03911-8.
[11] C.Y. Tso, K.C. Chan, C.Y.H. Chao, A field investigation of passive radiative cooling under Hong Kong's climate, Renew. Energy 106 (2017) 52–61, https://doi.org/10.1016/j.renene.2017.01.018.
[12] J. Liu, D. Zhang, S. Jiao, Z. Zhou, Z. Zhang, F. Gao, Preliminary study of radiative cooling in cooling season of the humid coastal area, Sol. Energy Mater. Sol. Cell. 208 (2020) 110412, https://doi.org/10.1016/j.solmat.2020.110412.
[13] Y. Yang, G. Zhang, L. Rong, Impact of cloud and total column water vapor on annual performance of passive daytime radiative cooler, Energy Convers. Manag. 273 (2022) 116420, https://doi.org/10.1016/j.enconman.2022.116420.
[14] J. Feng, M. Saliari, K. Gao, M. Santamouris, On the cooling energy conservation potential of super cool roofs, Energy Build. 264 (2022) 112076, https://doi.org/10.1016/j.enbuild.2022.112076.
[15] A. Baniassadi, D.J. Sailor, G.A. Ban-Weiss, Potential energy and climate benefits of super-cool materials as a rooftop strategy, Urban Clim. 29 (2019) 100495, https://doi.org/10.1016/j.uclim.2019.100495.
[16] L. Yang, J.C. Lam, C.L. Tsang, Energy performance of building envelopes in different climate zones in China, Appl. Energy 85 (2008) 800–817, https://doi.org/10.1016/j.apenergy.2007.11.002.
[17] T. Li, Y. Zhai, S. He, W. Gan, Z. Wei, M. Heidarinejad, et al., A radiative cooling structural material, Science 364 (2019) 760–763, https://doi.org/10.1126/science.aau9101.
[18] Z. Yi, Y. lv, D. Xu, J. Xu, H. Qian, D. Zhao, et al., Energy saving analysis of a transparent radiative cooling film for buildings with roof glazing, Energy and Built Environment 2 (2021) 214–222, https://doi.org/10.1016/j.enbenv.2020.07.003.
[19] J. Anand, D.J. Sailor, A. Baniassadi, The relative role of solar reflectance and thermal emittance for passive daytime radiative cooling technologies applied to rooftops, Sustain. Cities Soc. 65 (2021) 102612, https://doi.org/10.1016/j.scs.2020.102612.
[20] X. Li, B. Sun, C. Sui, A. Nandi, H. Fang, Y. Peng, et al., Integration of daytime radiative cooling and solar heating for year-round energy saving in buildings, Nat. Commun. 11 (2020) 6101, https://doi.org/10.1038/s41467-020-19790-x.
[21] X. Yu, C. Chen, Coupling spectral-dependent radiative cooling with building energy simulation, Build. Environ. 197 (2021) 107841, https://doi.org/10.1016/j.buildenv.2021.107841.
[22] K.W.D.K.C. Dahanayake, C.L. Chow, Studying the potential of energy saving through vertical greenery systems: using EnergyPlus simulation program, Energy Build. 138 (2017) 47–59, https://doi.org/10.1016/j.enbuild.2016.12.002.
[23] G. Fraisse, C. Viardot, O. Lafabrie, G. Achard, Development of a simplified and accurate building model based on electrical analogy, Energy Build. 34 (2002) 1017–1031, https://doi.org/10.1016/S0378-7788(02)00019-1.
[24] L. Vandenberghe, S. Boyd, A. El Gamal, Optimizing dominant time constant in RC circuits, IEEE Trans. Comput. Aided Des. Integrated Circ. Syst. 17 (1998) 110–125, https://doi.org/10.1109/43.681261.
[25] A. Berk, P. Conforti, R. Kennett, T. Perkins, F. Hawes, J. van den Bosch, MODTRAN® 6: a major upgrade of the MODTRAN® radiative transfer code, in: 2014 6th Workshop on Hyperspectral Image and Signal Processing: Evolution in Remote Sensing, WHISPERS, 2014, pp. 1–4, https://doi.org/10.1109/WHISPERS.2014.8077573.
[26] M. Martin, P. Berdahl, Characteristics of infrared sky radiation in the United States, Sol. Energy 33 (1984) 321–336, https://doi.org/10.1016/0038-092X(84)90162-2.
[27] H. Hersbach, B. Bell, P. Berrisford, G. Biavati, A. Horányi, J. Muñoz Sabater, J. Nicolas, C. Peubey, R. Radu, I. Rozum, D. Schepers, A. Simmons, C. Soci, D. Dee, J.-N. Thépaut, ERA5 hourly data on single levels from 1979 to present, Copernicus Climate Change Service (C3S) Climate Data Store (CDS) (2018), https://doi.org/10.24381/cds.adbb2d47 n.d.
[28] J. Liu, J. Zhang, D. Zhang, S. Jiao, Z. Zhou, H. Tang, et al., Theoretical and experimental research towards the actual application of sub-ambient radiative cooling, Sol. Energy Mater. Sol. Cell. 220 (2021) 110826, https://doi.org/10.1016/j.solmat.2020.110826.
[29] R. Karadağ, New approach relevant to total heat transfer coefficient including the effect of radiation and convection at the ceiling in a cooled ceiling room, Appl. Therm. Eng. 29 (2009) 1561–1565, https://doi.org/10.1016/j.applthermaleng.2008.07.005.
[30] J.R. Howell, M.P. Menguc, R. Siegel, Thermal Radiation Heat Transfer, 0 ed., CRC Press, 2010 https://doi.org/10.1201/9781439894552.
[31] L. Zhang, Y. Li, H. Zhang, X. Xu, Z. Yang, W. Xu, A review of the potential of district heating system in Northern China, Appl. Therm. Eng. 188 (2021) 116605, https://doi.org/10.1016/j.applthermaleng.2021.116605.
[32] J. Wu, C. Liu, H. Li, D. Ouyang, J. Cheng, Y. Wang, et al., Residential air-conditioner usage in China and efficiency standardization, Energy 119 (2017) 1036–1046, https://doi.org/10.1016/j.energy.2016.11.038.
[33] Y. Zhang, S. Hu, D. Yan, S. Guo, P. Li, Exploring cooling pattern of low-income households in urban China based on a large-scale questionnaire survey: a case study in Beijing, Energy Build. 236 (2021) 110783, https://doi.org/10.1016/j.enbuild.2021.110783.
[34] U.S. Department of energy, building energy codes program. https://www.energycodes.gov/development/commercial/prototype_models#90.1, 2020. (Accessed 25 September 2020). https://www.energycodes.gov/prototype-building-models#90.1. October 28, 2022.
[35] Intelligent Energy Europe Programme, TABULA-typology approach for building stock energy assessment, Available at, https://episcope.eu, 2021. (Accessed 1 September 2021), https://episcope.eu/welcome/. October 28, 2022.
[36] F. Johari, G. Peronato, P. Sadeghian, X. Zhao, J. Widén, Urban building energy modeling: state of the art and future prospects, Renew. Sustain. Energy Rev. 128 (2020) 109902, https://doi.org/10.1016/j.rser.2020.109902.
[37] T. Hu, H. Yoshino, Z. Jiang, Analysis on urban residential energy consumption of hot summer & cold winter zone in China, Sustain. Cities Soc. 6 (2013) 85–91, https://doi.org/10.1016/j.scs.2012.09.001.
[38] JGJ 134-2001 Design Standard for Energy Efficiency of Residential Buildings in Hot Summer and Cold Winter Zone, Standardization Administration of China, Beijing, China, 2001 (in Chinese). n.d.
[39] JGJ 134-2010 Design Standard for Energy Efficiency of Residential Buildings in Hot Summer and Cold Winter Zone, Standardization Administration of China, Beijing, China, 2010 (in Chinese). n.d.
[40] JGJ/T 449-2018 Standard for Green Performance Calculation of Civil Buildings, Standardization Administration of China, Beijing, China, 2018 (in Chinese). n.d.

[41] GB 50736-2012 Design Code for Heating Ventilation and Air Conditioning of Civil Buildings, Standardization Administration of China, Beijing, China, 2012 (in Chinese). n.d.
[42] GB 50352-2019 Uniform Standard for Design of Civil Buildings, Standardization Administration of China, Beijing, China, 2019 (in Chinese). n.d.
[43] D. van Dijk, EN ISO 52016 1: the new International Standard to calculate building energy needs for heating and cooling, internal temperature and heating and cooling loads, in: Proceedings of 16th IBPSA Conference, Rome, Italy, Sep 2-4, 2019, pp. 4061–4068.
[44] Yaoqing Lu, Practical Heating and Air Conditioning Design Manual, vol. 38, China Building Industry Press, 2008.
[45] A. Katal, M. Mortezazadeh, L Leon Wang, Modeling building resilience against extreme weather by integrated CityFFD and CityBEM simulations, Appl. Energy 250 (2019) 1402–1417, https://doi.org/10.1016/j.apenergy.2019.04.192.
[46] Z. Deng, Y. Chen, J. Yang, Z. Chen, Archetype identification and urban building energy modeling for city-scale buildings based on GIS datasets, Build Simul (2022), https://doi.org/10.1007/s12273-021-0878-4.
[47] GB/T 51161-2016 Standard for Energy Consumption of Buildings, Standardization Administration of China, Beijing, China, 2016 (in Chinese). n.d.